International Journal of Heat and Fluid Flow 78 (2019) 108423

Contents lists available at ScienceDirect

International Journal of Heat and Fluid Flow

journal homepage: www.elsevier.com/locate/ijhff

Contribution to tip leakage loss modeling in radial turbines based on 3D flow analysis and 1D characterization

José Ramón Serrano, Roberto Navarro, Luis Miguel García-Cuevas, Lukas Benjamin Inhestern*

CMT-Motores Térmicos, Universitat Politécnica de Valéncia, Valencia 46022, Spain

ARTICLE INFO

Keywords:
Tip leakage losses
Turbocharger
Radial turbines
Modeling
Radial turbine simulation
Off-design

ABSTRACT

The characterization of tip leakage flow plays an important role for one-dimensional loss modeling and design in radial turbine research. Tip leakage losses can be expressed as function of fluid momentum and mass flow passing through the tip gap. Friction-driven flow and contrariwise oriented pressure gradient-driven flow are highly coupled. However, these numbers are mostly unknown and dependent on tip gap geometry and turbine running condition. Based on a commonly used definition of a non-dimensional tip leakage momentum ratio, a novel correlation has been derived. This allows a consistent characterization for variable tip gap sizes over a wide range of operating conditions. The correlation has been validated by means of CFD data with high variety in reduced speed tip gap geometry and expansion ratios. Results of the novel number show significant improvements of quantitative and qualitative results over a wide range of running conditions in comparison to existing correlations. Furthermore, correlations for tip leakage velocities, that can easily be used in one-dimensional models, have been derived. Finally, it has been demonstrated, that the influence of inlet flow momentum on the tip leakage flow can be analyzed with presented correlations.

1. Introduction

While turbocharging is commonly used in conventional diesel engines to increase the intake pressure, it is more and more required for downsizing purposes in gasoline engines to meet increasingly tightened exhaust gas restrictions by governments worldwide. In the turbocharging system, the turbine experiences highly unsteady flow conditions in consequence of the pulsating flow generated by the cylinder exhaust of the reciprocating combustion engine. Furthermore, urban driving that gains continuously importance can lead to additional unsteadiness due to acceleration and deceleration of engine and turbocharger axis (EUR, 2007; Serrano et al., 2013). Thus, the turbine operates most of the time under off-design conditions (Galindo et al., 2013a), where the overall internal flow is rather unknown. As the turbine is attached to a compressor that acts as a brake with a very limited braking torque range at any given rotational speed, it is difficult to obtain measurements under these off-design conditions. However experimental procedures have been developed to measure in this zone (Romagnoli and Martinez-Botas, 2011; Salameh et al., 2016; Serrano et al., 2017c; 2017a), extended maps are not commonly available yet. Nevertheless, various extrapolation models have been published to extrapolate narrow measurement maps (Romagnoli and Martinez-Botas, 2011; Serrano et al., 2016; Baines, 1998). This kind of models often rely on submodels to estimate losses like passage or tip leakage losses.

Due to the typical small size of turbocharger radial turbines, they have rather high blade tip gap to blade tip radius ratios. These make the turbocharger turbine efficiency especially prone to tip leakage losses as confirmed by Kammeyer et al. (2010b). Hence, the modeling of the losses and a detailed knowledge of the main physical effects are of high interest for one dimensional modeling and turbine design. Due to the aforementioned off-design operation of the turbine, models valid over a wide range of operating conditions, from low pressure ratios to high pressure ratios and from low rotational speed to high rotational speed, are in demand. Several one-dimensional models predicting tip leakage losses have been published. The model introduced by Kammeyer et al. (2010a) is based on an empirical approach and is able to predict efficiency losses at design points dependent on geometrical information as the ratio of the tip gap to the tip width or to the rotor tip radius. The tip leakage loss model presented by Baines (2006) is widely used in one-dimensional turbocharger turbine modeling.

Dambach et al. (1998), Dambach and Hodson (2001) and Dambach et al. (2002) highlighted the importance of pressure-driven tip leakage flow and friction-driven tip leakage flow, which goes in opposing direction. Researchers, as in (Dambach et al., 1998; Yaras and

* Corresponding author.
E-mail address: luin@mot.upv.es (L.B. Inhestern).
URL: http://www.cmt.upv.es (L.B. Inhestern).

https://doi.org/10.1016/j.ijheatfluidflow.2019.108423
Received 10 October 2018; Received in revised form 13 February 2019; Accepted 21 May 2019

Nomenclature

Latin Letters

a	Fitting constant
b	Fitting constant
BSR	Blade Speed Ratio
c	Fitting constant
CFD	Computational Fluid Dynamics
dr	Radial integrator
g	Gravitational acceleration
h	Enthalpy
IGV	Inlet Guide Vane
i	Incidence
l	Length
La	Laval number
$\dot{m}$	Mass flow
M	Momentum
MAE	Mean Absolute Error
N	Rotational speed
NS	Navier Stokes equation
PS	Pressure Side
p	Pressure
R	Momentum ratio
r	Radius
RANS	Reynolds Averaged Navier Stokes
Re	Reynolds number
RMSE	Root Mean Square Error
SS	Suction Side
t	Time
T	Temperature
TE	Trailing Edge
VGT	Variable Geometry Turbine
$\dot{W}$	Power
w	Relative velocity
y^+	Non-dimensional wall distance
z	Blade number or z-coordinate

Subscripts

ax.	Axial component
eff.	Effective
filt.	Filtered
fl.	Fluid
geom.	Geometry
in	Inlet
mix	Mixed expression of fluid numbers and geometry
NS	Based on Navier Stokes equation
out	Outlet
r	Radial component
red.	Reduced numbers
s	Static conditions
sh.	Shroud
spec.	Specific
surf.	Value on surface
t	Total or stagnation conditions
tip	Blade tip
turb.	Turbine

Greek Letters

α	Stator blade angle
β	Incidence angle in rot. ref. frame
γ	Blade surface angle, isentropic exponent
Δ	Difference
∂	Increment
η	Efficiency
θ	Tangential component
π	Corresponding pressure ratio
σ	Blade speed ratio
ω	Angular velocity
ρ	Density
μ	Viscosity

Numbers and Symbols

0	Turbine inlet
+	Positive direction
-	Negative direction
-	Area average
$\perp$	Perpendicular

Sjolander, 1992), stated that the tip leakage related loss can mainly be correlated with the mass and momentum passing through the tip gap. Furthermore, it was shown that the ratio of pressure induced momentum to friction induced momentum can qualitatively predict locations of higher and lower efficiency losses over the tip. However, it has been shown that the proposed correlation for the momentum ratio underpredicts the values of momentum ratio, simulated by means of CFD, well below one order of magnitude (Serrano et al., 2018a). Missing geometrical variables also prevent to predict tip leakage flow precisely for changed geometries.

The consistent modeling of the reciprocal effect of opposing flow patterns in the tip region over wide range of speeds and blade loadings can be challenging. The physical model described in (Serrano et al., 2018b) can model tip leakage mass flow and momentum, which has further been correlated to obtain tip leakage losses for one-dimensional extrapolation models. While this model also relies on general geometrical information, it uses fitting coefficients to model the complex composition of contrarious fluid flows though the tip gap over a wide range of speeds and pressure ratios. Thus, an estimation of tip leakage flow losses for unmeasured geometries with varying tip gap heights and over a wide range of operating conditions is not possible yet. At the same time Peacock (Peacock, 1982; 1983) highlights the importance of the rotor tip gap height to the turbomachinery loss system.

The objective of this paper is to find aerodynamically-based correlations that can predict the momenta and velocities of friction and pressure induced flow for varying tip gap heights and for a wide range of operating conditions. These numbers are often required in one-dimensional loss modeling and further analysis. Therefore, the simulated data base has been presented and briefly analyzed. Following, the new correlation for the tip momentum ratio has been derived. Finally, results and possible fields of application are shown.

2. CFD setup & validation results

For the following analysis CFD results of wide range operating conditions by Serrano et al. (2017b) have been used as data basis. Further simulations have been executed to extend the available data. The analyzed turbine is a commonly sized turbocharger turbine with variable stator vanes. The geometrical details have been listed in Table 1 and related nomenclature of geometrical parameters have been shown in Fig. 1.

All simulations have been solved with the segregated solver of Star-CCM+ 12.04. Steady RANS simulations have been performed. Turbulence closure has been obtained by the kω-SST model

Table 1
Turbine geometry.

Stator	
Blade number	11
Blade angle α (VGT opening)	62.95° (60%)
Rotor	
Blade number	9
Inlet radius $r_{tip,in}$	20.05 mm
Outlet radius $r_{tip,out}$	19 mm
Outlet blade angle γ_{out}	59°
Inlet tip clearance $\Delta r_{tip,in}$	0.36 mm
Outlet tip clearance $\Delta r_{tip,out}$	0.4 mm
Axial tip clearance length ($l_{tip,ax.}$)	13 mm
Leading edge thickness $\Delta\theta$	0.0195 rad

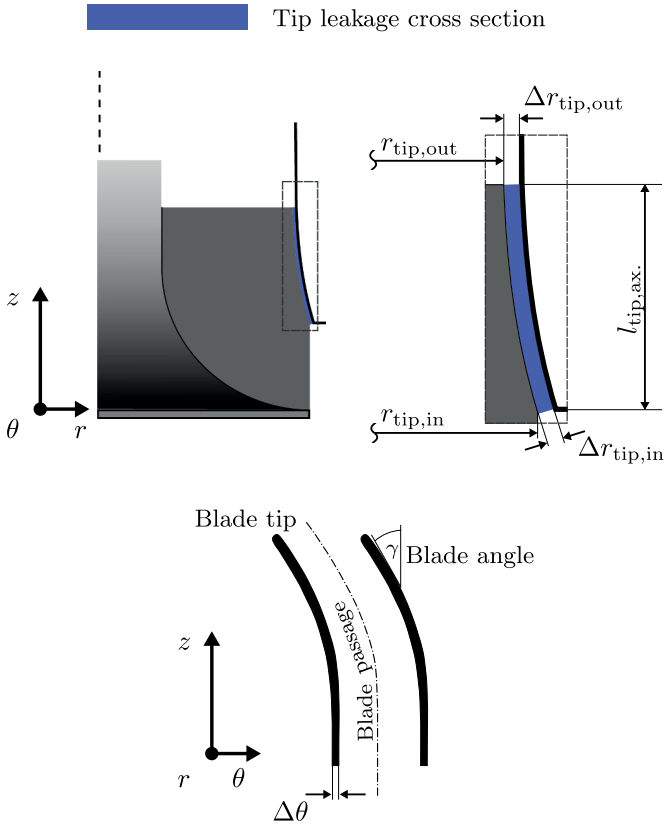

Fig. 1. Tip geometry nomenclature.

(Menter, 1994), which has been recommended in the literature for radial turbocharger simulations (Menter et al., 2004; Simpson et al., 2009; Galindo et al., 2013b). The simulations have been run with adiabatic walls. A polyhedral mesh with fine prism layer resolution on the wall has been used to resolve the boundary layer. The simulation setup to achieve CFD results at very low pressure ratios and a detailed mesh analysis have been elaborated in detail in (Serrano et al., 2017b) and are shown in Fig. 2. An overall y^+ value of around 1 has been obtained. The mesh convergence in the tip region was analyzed separately by doubling the mesh density without a considerable change in the tip leakage mass flow. In design conditions the negative leakage mass flow varies by 2.1% and the positive leakage mass flow by 1.3%. In off-design conditions variations are below 1%, when doubling the cells in the tip gap.

Simulations have been executed at four different speedlines from a low reduced speed of 1710 rpm/K$^{0.5}$ up to a high reduced speed of 6715 rpm/K$^{0.5}$ with the VGT opening set to 60%. Each speedline has been simulated over a wide range to get a complete picture of flow conditions that can occur during transient driving conditions. The tip gap height has been decreased by 50% and 25% (like it can appear due to heat expansion, centrifugal forces (Galindo et al., 2015), or different designs) % as it can be seen in Fig. 3. For the highest speed the tip gap height has also been increased by 50%. The original shroud has been maintained and only the rotor blades have been adjusted for this modification. Figs. 4 and 5 show respectively the simulated turbine efficiency, according to Eq. (1) and reduced turbine mass flow of simulated cases; both in comparison with experimentally obtained data.

$$\eta_{turb.} = \frac{T_{t,in} - T_{t,out}}{T_{t,in}\left[1 - \left(\frac{1}{\pi_{turb.}}\right)^{\frac{\gamma-1}{\gamma}}\right]} \quad (1)$$

The measurements have been done in quasi-adiabatic conditions and residual heat transfer was corrected by means of the model described in (Serrano et al., 2014). The experimental measurements in an extended range have been realized by using an IGV upstream the inlet of the compressor wheel to convert the compressor into a centrifugal turbine like it has been explained in (Serrano et al., 2017c). This way it was possible to maintain the rotational speed with power produced by the compressor wheel and to measure up to running points where the turbine even consumes energy and thus, works with negative efficiencies as they were reported by other researchers (Salameh et al., 2016; Serrano et al., 2017a; Terdich, 2015).

Experimental variations in the VGT positioning are inherent to the VGT moving mechanism. For the validation of the CFD method, the VGT opening was stepwise changed until the experimental mass flow was achieved in the running point of highest simulated pressure ratio at 3890 rpm/K$^{0.5}$ (Serrano et al., 2017b). As this procedure is time consuming and a changed geometry for each speed line is not desired for the analysis the VGT has been maintained at the same position. Keeping the adjusted VGT position for 3890 rpm/K$^{0.5}$ for the other simulated speeds might cause small differences between experimental and CFD model VGT opening. However, the qualitative behavior of efficiency and mass flow curves have been well reproduced by CFD over the entire range of the 3 highest speeds. At the lowest speed, efficiencies estimated by CFD are within the measurement errors, which are naturally high at points of low power output and small expansion ratios.

3. Tip leakage flow analysis

The comparison of CFD results with different tip gap heights in Fig. 4 and in Fig. 5 shows that this geometry change can influence significantly the turbine efficiency and rather less reduced mass flow. This has also been stated Kammeyer et al. (2010b). From the wide range data it can further be seen that the difference in efficiency diminishes towards very low pressure ratios/high BSRs with varying tip gap height. According to Dambach et al. (1998) the tip leakage flow is mainly dominated by pressure-driven leakage flow (positive direction in relative frame according to Fig. 6) and friction-driven flow through the tip gap (negative direction in relative frame according to Fig. 6). The CFD results are consistent with the observation that tip leakage mass flow in positive direction decreases due to lower blade loading. Nevertheless, the part of negative tip mass flow from the overall mass flow $\frac{\dot{m}_{tip,-}}{\dot{m}_{turb.}}$ increases towards operating conditions with low loads Serrano et al. (2018b). Thus, increasing parts of negative tip mass flow are not used for enthalpy extraction. This leads even to an increase of summed tip mass flows ($\dot{m}_{tip,+} + \dot{m}_{tip,-}$) in extreme off-design conditions.

In Figs. 7 and 8 profiles of specific mass flow in blade normal direction through the tip gap are shown for two running points (marked blue in Fig. 4 b) at 3890 rpm/K$^{0.5}$). The first shows a running point

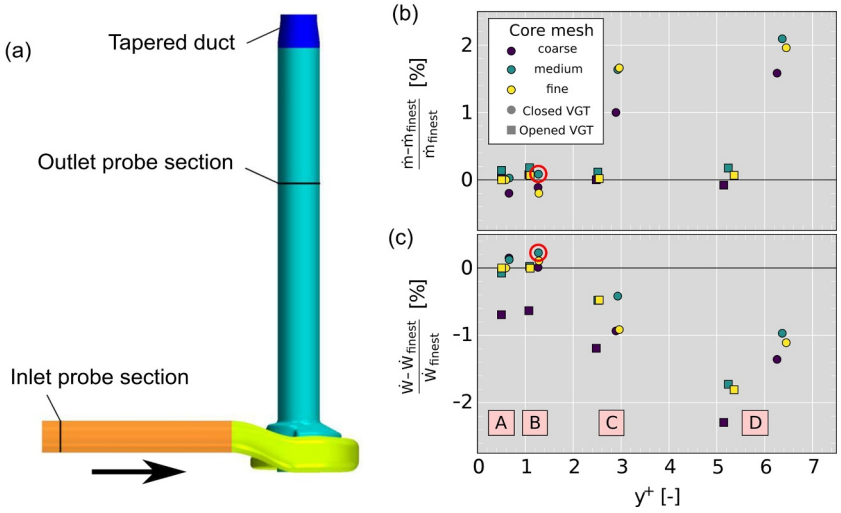

Fig. 2. (a): computational domain; (b) and (c): mesh convergence analysis. The red circle marks the chosen mesh for further executed simulations (Serrano et al., 2017b). (For interpretation of the references to colour in this figure legend, the reader is referred to the web version of this article.)

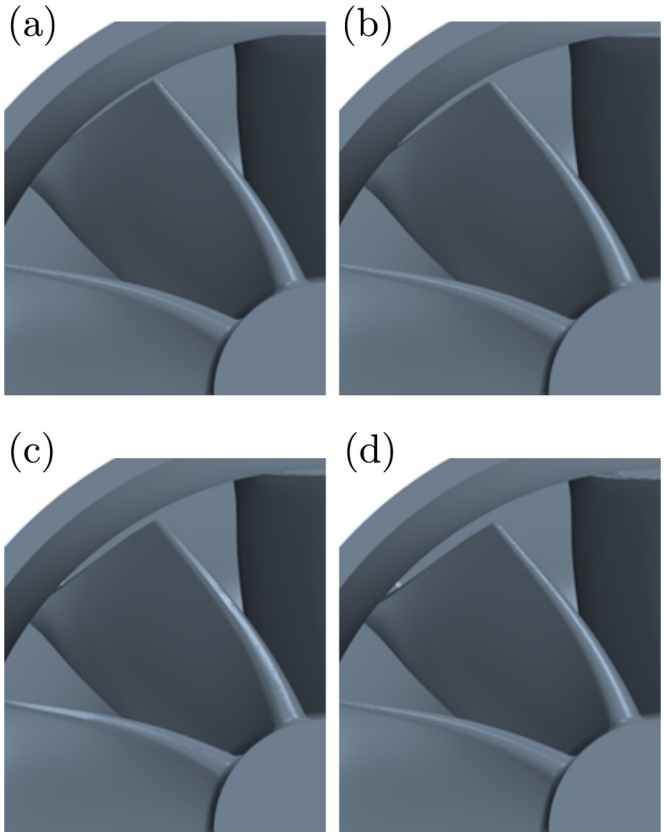

Fig. 3. Tip gap geometry variation: (a) 50% $\Delta r_{\text{tip,ref.}}$; (b) 75% $\Delta r_{\text{tip,ref.}}$; (c) 100% $\Delta r_{\text{tip,ref.}}$; (d) 150% $\Delta r_{\text{tip,ref.}}$.

close to design condition with low incidence. The later shows the flow at off-design condition and a high mean inflow incidence β of -51°. Since the flow profile close to design conditions looks rather undisturbed the diminishing influence of wall friction can be observed towards higher chord length. The higher radius in the inducer of the radial turbine causes faster relative shroud velocity. This generates a stronger fluid dragging effect in the inducer. Hence, the maximum specific mass flow increases continuously up to a chord length of around 0.7. Looking at the profiles in Fig. 8 a clear influence of the incidence flow can be seen. Maximums of positive specific mass flow seem to decrease by the opposing inflow momentum. On the one hand side, losses generated by positive tip flow might be reduced. On the other hand side, new losses are introduced by entropy increasing negative tip flow. Furthermore, the determination of related mass flow and momentum is rather challenging since the aforementioned effects are mixed. Due to the pulsating flow in a turbocharger turbine, the turbine can operate in zones of extremely high incidences. This and the complexity of the tip leakage flow at design and off-design conditions highlights the importance of understanding the dynamic of this loss generating process.

To calculate tip leakage losses several correlations are available. The tip loss coefficient Y in Eq. (2), that has been proposed by Yaras and Sjolander (1992), is widely used in the literature to correlate the relative tip velocity $w_{\text{tip, }\perp}$ with produced losses.

$$Y = \frac{l_{\text{tip}} \cdot \int 0.5 \cdot \rho \cdot w_{\text{tip},\perp} \cdot w_{\text{tip},\perp}^2 \, \mathrm{d}r}{\dot{m}_{\text{turb.}} \cdot \Delta h_0} \tag{2}$$

Following, correlations like the one in (Serrano et al., 2018b) were derived to calculate the overall relative tip loss:

$$\frac{\Delta h_{\text{tip}}}{h_{\text{t,0}}} = \frac{\dot{m}_{\text{tip,+}}}{\dot{m}_{\text{turb.}}} \cdot \frac{\gamma - 1}{\gamma + 1} \cdot La_{\text{tip,+}}^2 \cdot z + \frac{\dot{m}_{\text{tip,-}}}{\dot{m}_{\text{turb.}}} \cdot \frac{\gamma - 1}{\gamma + 1} \cdot La_{\text{tip,-}}^2 \cdot z. \tag{3}$$

Where La_{tip} is the corresponding tip gap Laval number with $\frac{w_{cl.,\vartheta}}{\sqrt{c_p \cdot T_{t,0}}}$. This can be integrated in the efficiency calculation of one-dimensional models as:

$$\eta_{\text{turb.}} = \left(\frac{\Delta h_{\text{t}}}{h_{\text{t,0}}} - \frac{\Delta h_{\text{tip}}}{h_{\text{t,0}}} \right) \cdot \left[1 - \left(\frac{1}{\pi_{\text{turb.}}} \right)^{\frac{\gamma - 1}{\gamma}} \right]^{-1}. \tag{4}$$

This leads to the need of consistent and reliable correlations for tip leakage momentum and mass flow.

4. Method for tip leakage flow characterization

Dambach et al. (1998) showed that the specific momentum ratio of positive and negative momentum behaves qualitatively similar to the loss coefficients Y over the chord length. Furthermore, similar magnitudes and qualitative behavior along the chord length have been stated for conventional radial turbines and turbocharger turbines (Kammeyer et al., 2010a; Dambach et al., 1998). It has been recommended to formulate the momentum ratio of both leakage flows for characterizing tip

flow as:

$$R = \frac{M_{\mathrm{tip},+}}{M_{\mathrm{tip},-}} = \frac{\Delta p_{(\mathrm{PS,SS})}}{\rho\omega^2 r_{\mathrm{sh.}}^2 \cos\gamma^2}. \tag{5}$$

Here, the only needed fluid number is the surface pressure difference between SS and PS close to the wall, which makes this number easy to use. However, the proposed ratio misses important information of tip leakage dimensions.

For one dimensional modeling and for design purposes it can be important to distinguish friction and pressure driven effects in the tip leakage flow from other effects as incidence flow or blow by. Thus, to be able to estimate the quantity of this loss generating flow phenomena dependent on geometrical details is of interest. The aforementioned momentum ratio correlates qualitatively well along the chord length with estimated loss productions but misses to predict the qualitative change in momentum ratio when the geometry is changed (Serrano et al., 2018a). Following, the correlation of both momentum flows has newly been derived.

4.1. Novel momentum ratio

Conventional radial turbines operate mostly under design conditions, where it is reported to have most of the tip leakage losses in the radial tip gap in the exducer part (Dambach et al., 1998). Additionally, radial turbocharger turbines barely own an axial tip gap as it can be seen in Fig. 1. Hence, the circumferential momentum equation of the Navier Stokes equations (NS) in a cylindrical rotational reference frame Eq. (6) has been simplified under the assumptions: $\frac{\partial}{\partial t}$, $\frac{\partial}{\partial \theta}$, $\frac{\partial}{\partial z}$, $w_{\mathrm{r}} = 0$.

$$\begin{aligned}\rho\left(\frac{\partial w_\Theta}{\partial t} + w_{\mathrm{r}}\frac{\partial w_\Theta}{\partial r} + \frac{w_\Theta}{r}\frac{\partial w_\Theta}{\partial \theta} + \frac{w_{\mathrm{r}} w_\Theta}{r} + w_{\mathrm{z}}\frac{\partial w_\Theta}{\partial z}\right) = \\ -\frac{1}{r}\frac{\partial p}{\partial \theta} + \rho g_\Theta - 2\rho\omega w_{\mathrm{r}} \\ +\mu\left[\frac{1}{r}\frac{\partial}{\partial r}\left(r\frac{\partial w_\Theta}{\partial r}\right) - \frac{w_\Theta}{r^2} + \frac{1}{r^2}\frac{\partial^2 w_\Theta}{\partial \theta^2} + \frac{2}{r^2}\frac{\partial w_{\mathrm{r}}}{\partial \theta} + \frac{\partial^2 w_\Theta}{\partial z^2}\right]\end{aligned} \tag{6}$$

Based on these assumptions and a calculation applying various substitutions, solving the resulting inhomogeneous differential equation with non-constant coefficients and integrating over the tip gap leads an analytical function for the tangential velocity profile over the radius. Terms including the pressure gradients and the friction driving shroud velocity have been separated to simplify the correlations. This way both flow effects have been decoupled first. Following, integration over the tip gap height and averaging leads to Eqs. (7) and (8). The derivation has been done in (Serrano et al., 2018b).

$$\begin{aligned}\bar{w}_{\mathrm{tip},\vartheta,+} = \Bigg\{\left[\frac{r_{\mathrm{tip}}^2 - r_{\mathrm{sh.}}^2}{4} + \frac{r_{\mathrm{sh.}}^2}{2}\cdot\ln\left(\frac{r_{\mathrm{sh.}}}{r_{\mathrm{tip}}}\right)\right] \\ - \frac{\left[\frac{r_{\mathrm{sh.}}^2 - r_{\mathrm{tip}}^2}{2\cdot r_{\mathrm{tip}}^2} + \ln\left(\frac{r_{\mathrm{tip}}}{r_{\mathrm{sh.}}}\right)\right]}{\left(\frac{r_{\mathrm{sh.}}}{r_{\mathrm{tip}}^2} - \frac{1}{r_{\mathrm{sh.}}}\right)}\cdot\left[r_{\mathrm{sh.}}\ln\left(\frac{r_{\mathrm{sh.}}}{r_{\mathrm{tip}}}\right)\right]\Bigg\}\cdot\frac{1}{2}\frac{1}{\mu}\frac{\Delta p_{(\mathrm{PS,SS})}}{\Delta\theta\Delta r_{\mathrm{tip}}}\end{aligned} \tag{7}$$

$$\bar{w}_{\mathrm{tip},\vartheta,-} = \frac{\left[\frac{r_{\mathrm{sh.}}^2 - r_{\mathrm{tip}}^2}{2\cdot r_{\mathrm{tip}}^2} + \ln\left(\frac{r_{\mathrm{tip}}}{r_{\mathrm{sh.}}}\right)\right]}{\left(\frac{r_{\mathrm{sh.}}}{r_{\mathrm{tip}}^2} - \frac{1}{r_{\mathrm{sh.}}}\right)}\cdot\frac{\omega\cdot r_{\mathrm{sh.}}\cdot\cos\gamma}{\Delta r_{\mathrm{tip}}} \tag{8}$$

Here, the leading effects of wall friction and pressure difference between SS and PS have already been separated to model the mean relative velocity of the negative and positive tip leakage flow. Furthermore, the geometrical terms (including $r_{\mathrm{sh.}}$ and r_{tip}) have been concentrated into one factor. Next, the momentum ratio has been defined as:

$$R_{\mathrm{NS}} = \frac{\rho_+}{\rho_-}\cdot\frac{\bar{w}_{\mathrm{tip},\vartheta,+}^2}{\bar{w}_{\mathrm{tip},\vartheta,-}^2} \tag{9}$$

Substituting Eqs. (7) and (8) in Eq. (9) the novel momentum ratio can be described as:

$$\begin{aligned}R_{\mathrm{NS}} = \frac{\rho_+}{\rho_-}\cdot\Bigg\{\frac{\left(\frac{r_{\mathrm{sh.}}}{r_{\mathrm{tip}}^2} - \frac{1}{r_{\mathrm{sh.}}}\right)\left[\frac{r_{\mathrm{tip}}^2 - r_{\mathrm{sh.}}^2}{4} + \frac{r_{\mathrm{sh.}}^2}{2}\cdot\ln\left(\frac{r_{\mathrm{sh.}}}{r_{\mathrm{tip}}}\right)\right]}{\left[\frac{r_{\mathrm{sh.}}^2 - r_{\mathrm{tip}}^2}{2\cdot r_{\mathrm{tip}}^2} + \ln\left(\frac{r_{\mathrm{tip}}}{r_{\mathrm{sh.}}}\right)\right]r_{\mathrm{sh.}}} \\ - \ln\left(\frac{r_{\mathrm{sh.}}}{r_{\mathrm{tip}}}\right)\Bigg\}^2\left\{\frac{\frac{1}{2}\frac{1}{\mu}\frac{\Delta p_{(\mathrm{PS,SS})}}{\Delta\theta}}{\omega\cos\gamma}\right\}^2\end{aligned} \tag{10}$$

It can be seen that only the viscosity and the pressure on SS and PS are required from the flow to calculate the ratio. The viscosity has been assumed to be constant here. For the purpose of simplicity and for later analysis the following nomenclature has been chosen for the purely geometry dependent factor and the "fluid" factor:

$$R_{\mathrm{geo.}} = \left\{\frac{\left(\frac{r_{\mathrm{sh.}}}{r_{\mathrm{tip}}^2} - \frac{1}{r_{\mathrm{sh.}}}\right)\left[\frac{r_{\mathrm{tip}}^2 - r_{\mathrm{sh.}}^2}{4} + \frac{r_{\mathrm{sh.}}^2}{2}\cdot\ln\left(\frac{r_{\mathrm{sh.}}}{r_{\mathrm{tip}}}\right)\right]}{\left[\frac{r_{\mathrm{sh.}}^2 - r_{\mathrm{tip}}^2}{2\cdot r_{\mathrm{tip}}^2} + \ln\left(\frac{r_{\mathrm{tip}}}{r_{\mathrm{sh.}}}\right)\right]r_{\mathrm{sh.}}} - \ln\left(\frac{r_{\mathrm{sh.}}}{r_{\mathrm{tip}}}\right)\right\}^2 \tag{11}$$

$$R_{\mathrm{fl.}} = \left\{\frac{\frac{1}{2}\frac{1}{\mu}\frac{\Delta p_{(\mathrm{PS,SS})}}{\Delta\theta}}{\omega\cos\gamma}\right\}^2 \tag{12}$$

$$R_{\mathrm{NS}} = \frac{\rho_+}{\rho_-}\cdot R_{\mathrm{geom.}}\cdot R_{\mathrm{fl.}} \tag{13}$$

It is worth highlighting that $R_{\mathrm{fl.}}$ would result in extremely high values, if $\Delta\theta$ would be defined by the small blade thickness. This might be the case because $\frac{\partial}{\partial\theta} = 0$ has been assumed deriving the final equations. This is an assumption for developed flow, which is apparently not the case after the short distance of a tip gap. However, this assumption overcomes estimating a flow profile at tip gap inlet to obtain a gap flow profile at the outlet and makes the solution of the Navier Stokes equation much easier, while maintaining the main trends. Thus, $\Delta\theta$ must be understood as an effective flow length $\Delta\theta_{\mathrm{eff.}}$ and has been analyzed in more detail.

4.2. Effective flow length

The momentum ratio obtained from the CFD simulations has been used to calculate the effective flow length and the chordwise distributions of $\Delta p_{(\mathrm{PS,SS})}$ values from the CFD results have been imposed:

$$\Delta\theta_{\mathrm{eff.}} = \sqrt{\frac{\rho_+}{\rho_-}\cdot\frac{R_{\mathrm{geom.}}}{R_{\mathrm{CFD}}}}\cdot\frac{\frac{1}{2}\frac{1}{\mu}\Delta p_{(\mathrm{PS,SS})}}{\omega\cos\gamma}. \tag{14}$$

Here, the simulated momentum ratio R_{CFD} has following been calculated by:

$$R_{\mathrm{CFD}} = \frac{M_{\mathrm{tip,spec.},+}}{M_{\mathrm{tip,spec.},-}}. \tag{15}$$

Further, the simulated specific momentum trough the tip gap over a line at constant chord length has been processed from the CFD data according to Eqs. (16) and (17) in positive and negative direction:

$$M_{\mathrm{tip,spec.},+} = \int_{r_{\mathrm{tip}}}^{r(w_{\mathrm{tip},\perp}=0)} \rho\cdot w_{\mathrm{tip},\perp}\cdot w_{\mathrm{tip},\perp}\,\mathrm{d}r, \tag{16}$$

$$M_{\mathrm{tip,spec.},-} = \int_{r(w_{\mathrm{tip},\perp}=0)}^{r_{\mathrm{sh.}}} \rho\cdot w_{\mathrm{tip},\perp}\cdot w_{\mathrm{tip},\perp}\,\mathrm{d}r. \tag{17}$$

$\Delta\theta_{\mathrm{eff.}}$ is expected to behave as the discharge coefficient appearing in publications about flow characterization of flow through an orifice

(Borutzky et al., 2002) and thus, can be characterized by means of the Reynolds numbers of both flow directions:

$$Re_{+} = \frac{\rho_{+} \cdot \bar{w}_{\mathrm{tip},\theta,+} \cdot \Delta r_{\mathrm{tip}}}{\mu}, \tag{18}$$

$$Re_{-} = \frac{\rho_{-} \cdot \omega \cdot r_{\mathrm{sh.}} \cdot \Delta r_{\mathrm{tip}} \cdot \cos\gamma}{\mu}. \tag{19}$$

It has been found out that plotting $\Delta\theta_{\mathrm{eff.}}$ over the ratio $\frac{Re_{-}}{Re_{+}^{1/6}}$ gives a clear trend for all simulated points as Fig. 9 shows. Here, average values from 0% to 100% chord length have been used to reduce complexity. Towards off-design condition the aforementioned influence of the incidence flow momentum on the momentum ratio causes higher values of the mean effective inflow length and explains the deviation from the overall trend for those points. The global trend is independent of the tip gap height Δr_{tip}, the rotational speed $N_{\mathrm{red.}}$ and of the overall turbine pressure ratio $\pi_{\mathrm{turb.}}$. It is worth highlighting, that the consistent line fitting can allow a correlation fit based on only a few data points of one single tip gap geometry. With this fitting results can be extrapolated towards different tip gap values.

Since friction and pressure driven effects have been decoupled to obtain the ratio R_{NS}, the relation in Fig. 9 represents the coupling of both flows due to fluid friction. $\Delta\theta_{\mathrm{eff.}}$ is increasing with rising rotational speed (increase of friction layer and reduction of effective area for pressure driven flow) and is decreasing when $\pi_{\mathrm{turb.}}$ (and thus $\Delta p_{(\mathrm{PS,SS})}$) is increasing. The working principle of $\Delta\theta_{\mathrm{eff.}}$ is similar to the one of combined discharge coefficients of both tip leakage flows. However, in contrast to discharge coefficients, $\Delta\theta_{\mathrm{eff.}}$ is not related to the tip gap height. This conserves the valuable trends inherent in $R_{\mathrm{geom.}}$. Apparently, the relation of $\Delta\theta_{\mathrm{eff.}}$ is dependent on itself, when Eq. (18) is calculated with the proposed formula in Eq. (7):

$$\Delta\theta_{\mathrm{eff.}} = f\left(\frac{Re_{-}}{f(\Delta\theta_{\mathrm{eff.}})}\right). \tag{20}$$

The data can directly be fitted with an exponential equation as it can be seen in Fig. 9. However, this would only allow an iterative solution, what causes difficulties in the further analysis and conclusions. Since an analytical solution is aimed $\Delta\theta_{\mathrm{eff.}}$ has been fitted with a simple parabolic function:

$$\Delta\theta_{\mathrm{eff.}} = a \cdot \left(\frac{Re_{-}}{Re_{+}^{1/6}}\right)^{b}. \tag{21}$$

Following, the analytical solution of R_{NS} can be obtained by substituting Eqs. (21), (18), (19) in Eq. (10) and considering $\Delta\theta$ as $\Delta\theta_{\mathrm{eff.}}$:

$$R_{\mathrm{NS}} = a^{\frac{12}{6-b}} \cdot \frac{\rho_{+}}{\rho_{-}} \cdot R_{\mathrm{fl.,eff.}} \cdot R_{\mathrm{mix,eff.}} \cdot R_{\mathrm{geom.,eff.}}$$

with:

$$R_{\mathrm{fl.,eff.}} = \left(\frac{1}{2}\frac{1}{\mu}\frac{\Delta p_{(\mathrm{PS,SS})}}{\omega\cos\gamma}\right)^{\frac{12}{6-b}},$$

$$R_{\mathrm{mix,eff.}} = \left(\frac{\rho_{+}}{\rho_{-}^{6}}\right)^{\frac{2\cdot b}{6-b}} \cdot \left\{\frac{\mu^{5}}{(\cos\gamma\cdot\omega)^{5}}\right\}^{\frac{2\cdot b}{6-b}} \cdot \left(\frac{1}{\Delta r_{\mathrm{tip}}^{5} \cdot r_{\mathrm{sh.}}^{5}}\right)^{\frac{2\cdot b}{6-b}},$$

$$R_{\mathrm{geom.,eff.}} = R_{\mathrm{geom.}}^{\frac{6}{6-b}} \cdot \left\{\frac{\left[\frac{r_{\mathrm{sh.}}^{2} - r_{\mathrm{tip}}^{2}}{2\cdot r_{\mathrm{tip}}^{2}} + \ln\left(\frac{r_{\mathrm{tip}}}{r_{\mathrm{sh.}}}\right)\right]}{\left(\frac{r_{\mathrm{sh.}}}{r_{\mathrm{tip}}^{2}} - \frac{1}{r_{\mathrm{sh.}}}\right)\Delta r_{\mathrm{tip}}}\right\}^{\frac{2\cdot b}{6-b}}. \tag{22}$$

It can be seen that the factor $R_{\mathrm{geom.}}$ has been extended and changes its exponent as well as $R_{\mathrm{fl.}}$. Additionally, a third non-dimensional factor $R_{\mathrm{mix.,eff.}}$ arises. This factor consists of geometry data and fluid information to model and is needed (together with aforementioned modifications of the equation) to model the interaction between wall friction flow and pressure-driven flow.

5. Model results & discussion

5.1. Model fitting

By means of a nonlinear fitting the MATLAB coded model has been fitted towards the chordwise R_{CFD} values of all simulated points including all tip gap configurations. Also here, the chordwise distributions of $\Delta p_{(\mathrm{PS,SS})}$ from the CFD results have been utilized. Simulation results have shown that the density ratio is close to 1. The fitting coefficients have been obtained as $a = 1250$ and $b = 1.23$. The average fitting error in R_{NS} is relatively low with 3.19 and the RMSE has been determined as 6.36. Mean values of each tip gap and running point of R_{CFD} have been reproduced in good quality for the most of the analyzed points as it can be seen in Fig. 10. The two outliers in Fig. 10 are those of highest mass flow $\dot{m}_{\mathrm{red.,turb.}}$ and biggest tip gap configuration. In these conditions the proposed model underestimates the mean momentum ratio $\bar{R}_{\mathrm{NS}}$. This could be caused by operation at high mass flow rates and following, higher simulated passage flow momentum passing through the tip gap.

Since the momentum through the tip gap can be related with the tip clearance losses and good fitting quality has been achieved for mean values of R_{NS}, the presented correlation might help to further reduce the number of fitting coefficients in one dimensional tip leakage models like the one described in (Serrano et al., 2018b). Furthermore, the dependence on the geometry as blade angle γ, blade radius r_{tip}, and tip gap height Δr_{tip} allows to increase model sensibility for the analysis and prediction of the tip leakage flow and losses for a bigger range of unmeasured geometries.

Apart from the capability to obtain good estimations for the mean value of R_{NS}, the fitted model can be applied to do further qualitative analysis. In Fig. 11 it can be seen that the ratio R_{NS} is well predicted over the chord length for the 50%, 75%, and the 100% tip gap configuration. R_{NS} is able to catch the high momentum ratio reduction close to 0, at lower relative chord lengths, that R was not able to predict (Serrano et al., 2017b). Table 2 shows the fitting quality for each tip gap configuration. As it can be seen, that the fitting quality is the best for the smallest tip gap and worsens continuously with opening the tip gap. The chordwise fitting becomes bad for the biggest tip gap of 150%. As mentioned before, the characteristic tip leakage flow with the biggest tip gap is affected by unguided passage flow momentum. This effect cannot be predicted by the model, since the model only considers blade loading and friction-driven flow. Although this represents a limitation of the chordwise modeling, such values of the tip gap heights are technically less relevant because the tip gap in real working conditions is reduced. In Fig. 12 pressure profiles for the red circles marked running points of Fig. 4(d) have been presented over the chord length. The pressure profile changes rather less when the gap height is reduced from 100% over 75% to 50%. At the same time blade loading at the tip cannot be conserved in the same quality when the tip gap is 50% increased.

Concluding, the modeled momentum ratio R_{NS} is able to reproduce the following trend: there are higher parts of pressure-driven momentum flows through the tip gap, when the tip gap becomes bigger, even when the blade loading changes only slightly or decreases.

5.2. Momentum ratio analysis

While a non-dimensional analysis of the factor $R_{\mathrm{fl.,eff.}}$ requires further assumptions of the blade loading or rotational speed, the newly gained factors $R_{\mathrm{geom.,eff.}}$ of Eq. (22) can be analyzed only dependent on geometry variations. Since the mixed ratio $R_{\mathrm{mix,eff.}}$ has further variables as density ratio, blade angle correlations and radial velocity, assumptions and simplifications have had to be made for continuing the analysis. While the impact of the density and the blade angle have been neglected here (= 1), a constant angle velocity of 14963 rad/s (U_{in} = 300 m/s) has been assumed. For analyzing the overall impact of

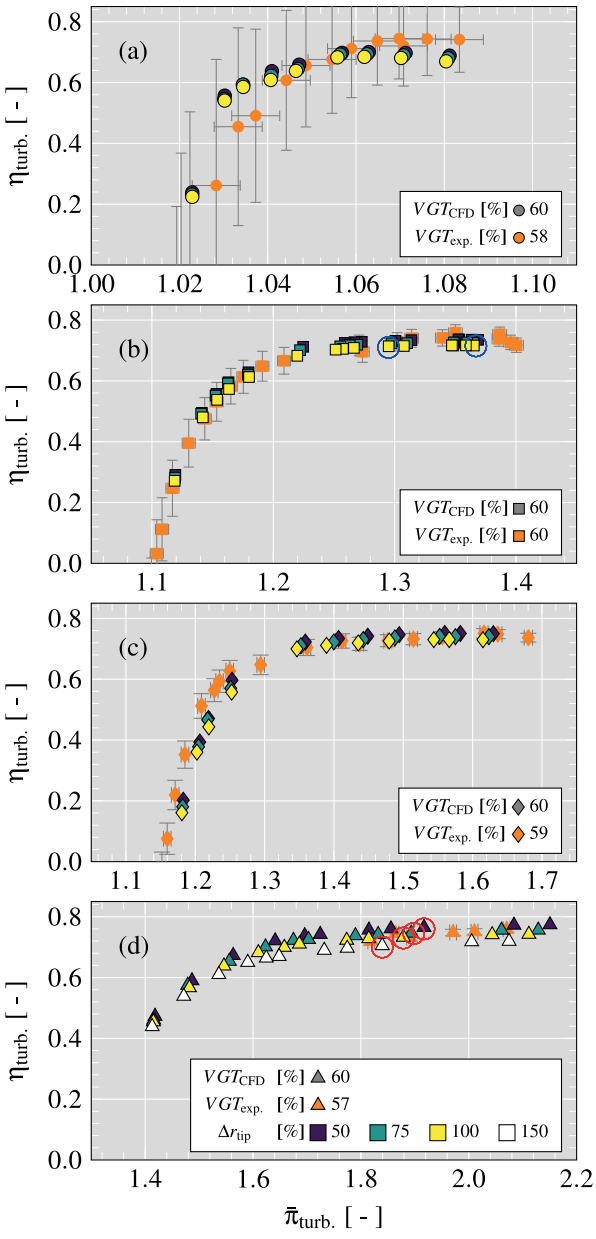

Fig. 4. Efficiency of simulated and measured running points at: (a) 1710 rpm/$K^{0.5}$; (b) 3890 rpm/$K^{0.5}$; (c) 4890 rpm/$K^{0.5}$; (d) 6715 rpm/$K^{0.5}$. The color code for different Δr_{tip} configurations in (d) is also valid in the other subplots.

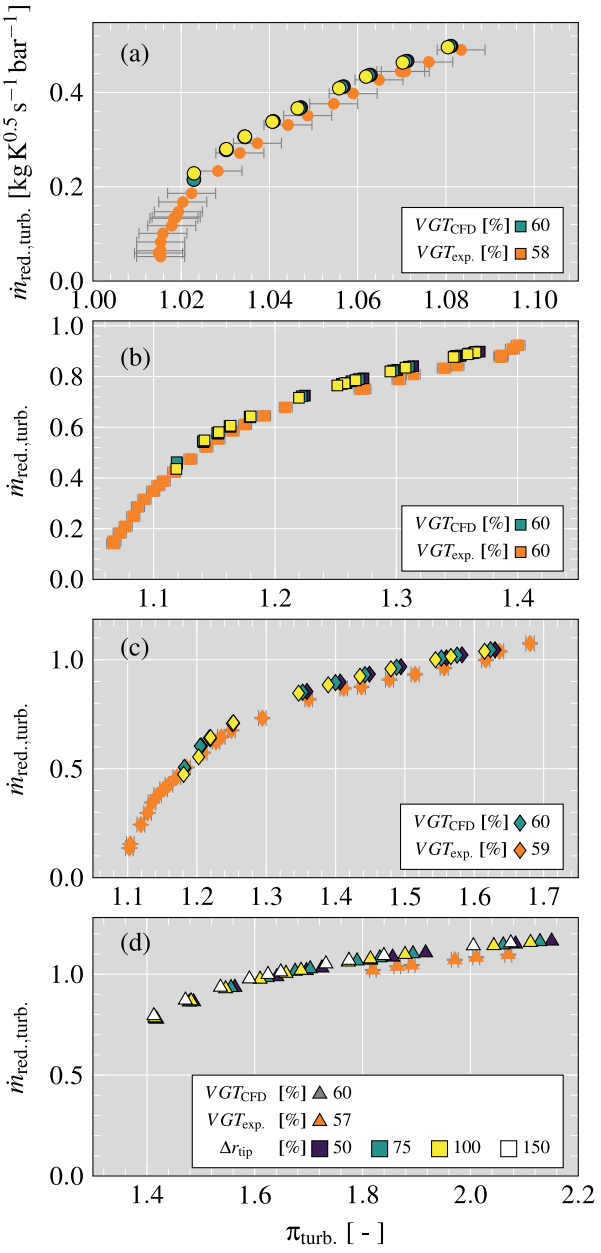

Fig. 5. Reduced mass flow of simulated and measured running points at: (a) 1710 rpm/$K^{0.5}$; (b) 3890 rpm/$K^{0.5}$; (c) 4890 rpm/$K^{0.5}$; (d) 6715 rpm/$K^{0.5}$. The color code for different Δr_{tip} configurations in (d) is also valid in the other subplots.

geometry changes on the momentum ratio, the newly gained ratio $R_{mix,eff.}$ with the aforementioned assumptions has been multiplied with $R_{geom.,eff.}$ as it can be seen in Fig. 13. The factor $R_{geom.,eff.} \cdot R_{mix,eff.}$ increases exponentially with decreasing tip radius r_{tip} and increasing $\frac{\Delta r_{tip}}{r_{tip}}$. This confirms independent from the factor $R_{fl.,eff.}$, which includes local blade loading and rotational speed, a tendency to higher positive leakage momentum and related losses at lower radius. Thus, front loaded blade designs are also in turbocharger turbines without axial tip gap in favor of a minimization of tip leakage losses. Finally, Fig. 14 shows the entire ratio of Eq. (22) in dependence of the variables ω and $\Delta p_{(PS,SS)}$, which are defining $R_{fl.}$. As geometry input for r_{tip}, $r_{sh.}$, and $cos\gamma$ constant values have been set. Here, the geometry of the chord length with highest blade loading that has been found for the most CFD solutions has been taken (with Δr_{tip} = 100%). The highest blade loading occurs mostly close to 60% chord length, in the exducer section. Also, the highest found blade loading for each simulated running point has been shown against the radial velocity to highlight the simulated

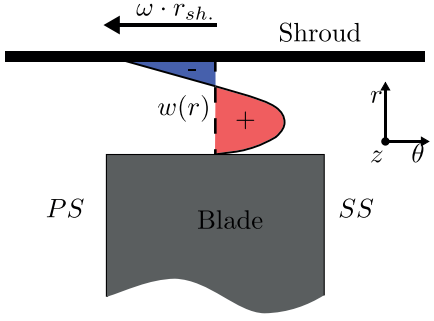

Fig. 6. Definition of positive and negative tip flow.

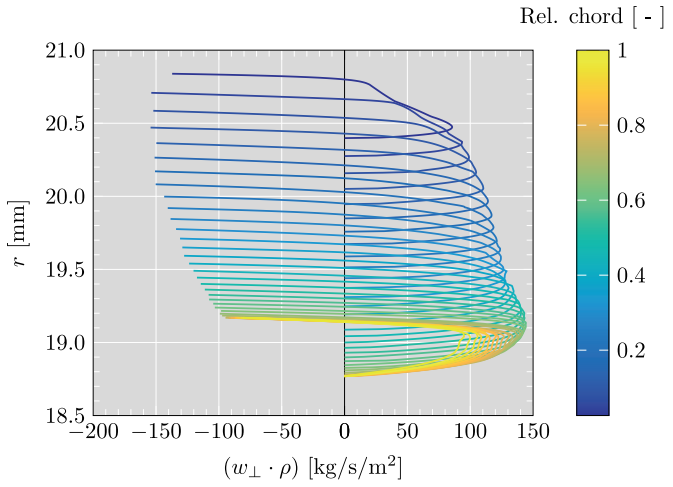

Fig. 7. Tip leakage flow profiles of low negative incidence inlet flow over the tip gap at 3890rpm/K$^{0.5}$ and a $\pi_{\text{turb.}}$ of 1.37.

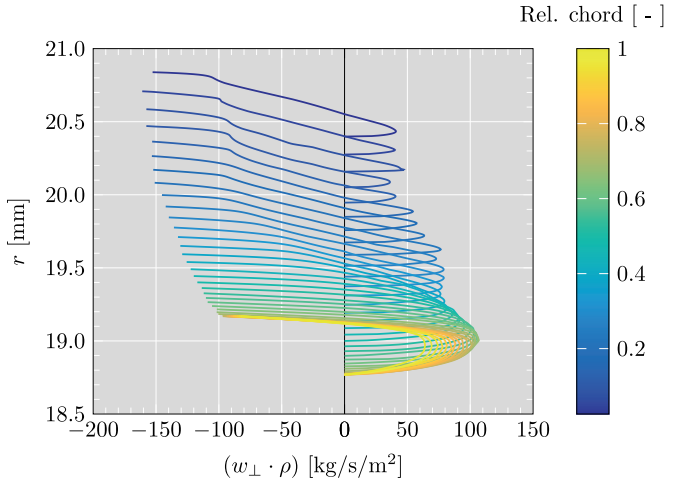

Fig. 8. Tip leakage flow profiles of high negative incidence inlet flow over the tip gap at 3890rpm/K$^{0.5}$ and a $\pi_{\text{turb.}}$ of 1.29.

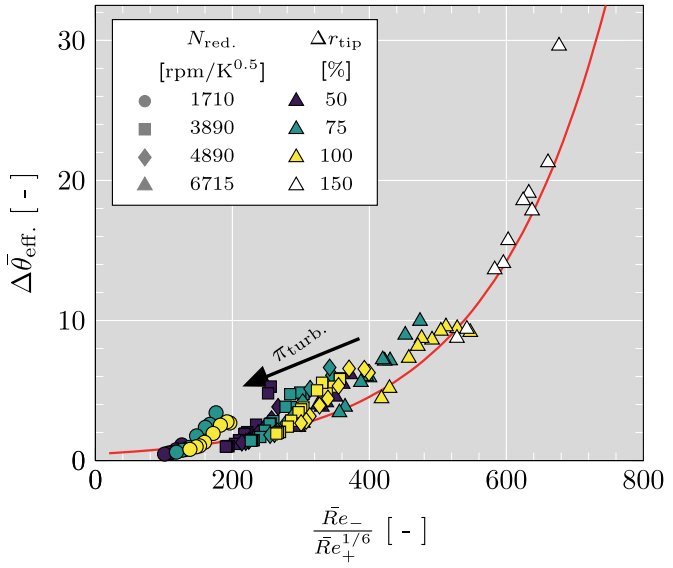

Fig. 9. Fitting of $\Delta\bar{\theta}_{\text{eff.}}$ values.

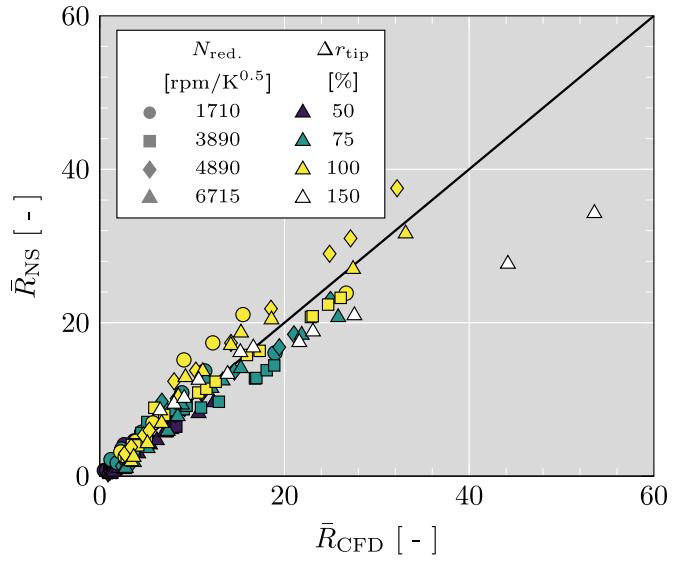

Fig. 10. Mean values for momentum ratio R_{NS} with simple exponential function (Eq. (21)).

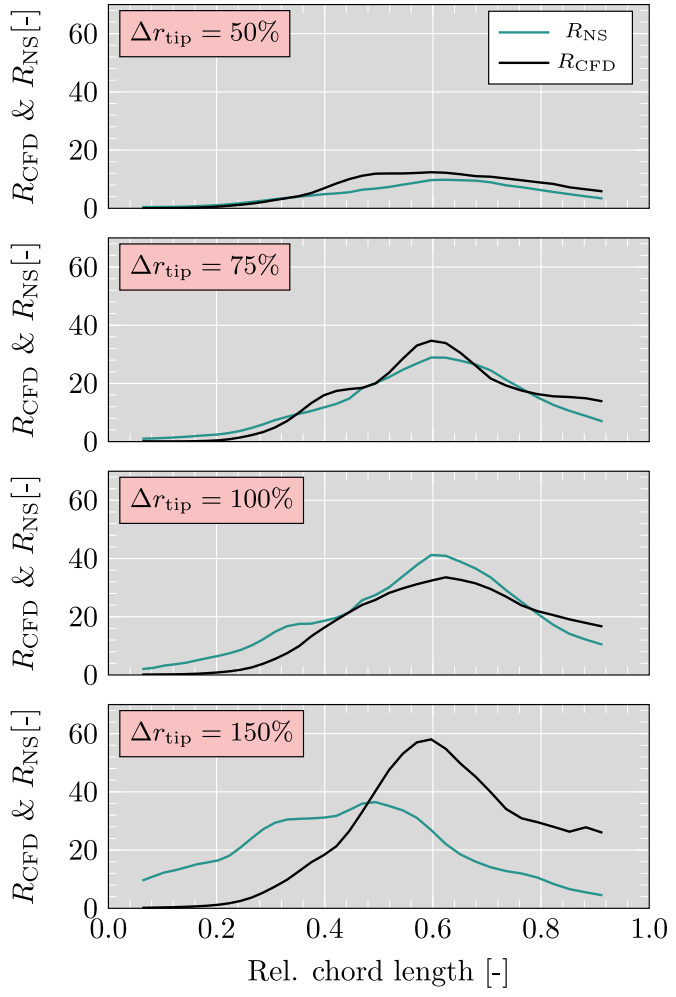

Fig. 11. Momentum ratios R_{CFD} (Eq. (15)), and R_{NS} (Eq. (22)) for four different tip gap heights at 6715 rpm/K$^{0.5}$ and 60% VGT opening (red circles in Fig. 4(d)). (For interpretation of the references to colour in this figure legend, the reader is referred to the web version of this article.)

Table 2
Fitting quality for each tip gap configuration.

Δr_{tip}	50%	75%	100%	150%
MAE	1.07	2.33	3.16	14.80
RMSE	1.52	3.31	4.14	19.78

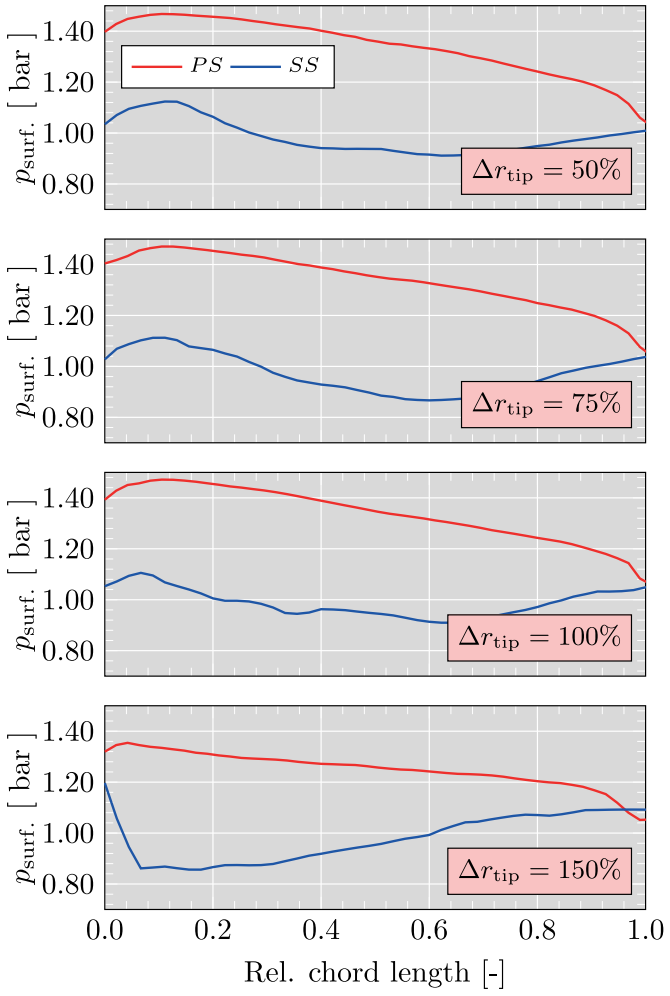

Fig. 12. Surface pressure profiles at 95% span for four different tip gap geometries at 6715 rpm/K$^{0.5}$ and 60% VGT opening (red circle in Fig. 4(d)). (For interpretation of the references to colour in this figure legend, the reader is referred to the web version of this article.)

operating range and relevant values for R_{NS}. To evaluate the validity of the presented model results, a comparison of the momentum ratios $R_{CFD,\Delta p\,max}$ and $R_{NS,\Delta p\,max}$ at described location has been shown in Fig. 14. The given trends are well reproduced by the found correlation.

In Fig. 14 it can be seen that each simulated speed covers a similar range of R_{NS} from low values (1.7–5.3) up to values around 40 and higher. While the momentum ratio is changing rather less at off-design conditions with lower blade loading, a small increase in the local blade loading $\Delta p_{(PS,SS)}$ can cause a significant increase of the momentum ratio and thus, of the tip leakage losses when operating at high efficiencies and close to design condition. This inherent sensitivity of the tip leakage momentum ratio on $\Delta p_{(PS,SS)}$ highlights, why the model results at nearly design condition in Fig. 11 can be considered as relatively good.

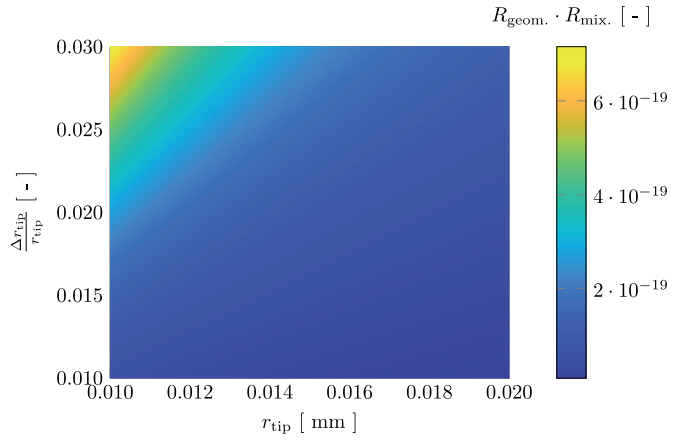

Fig. 13. Geometry changes vs. geometrical factor $R_{geom.,eff.}$ times mixed factor $R_{mix,eff.}$.

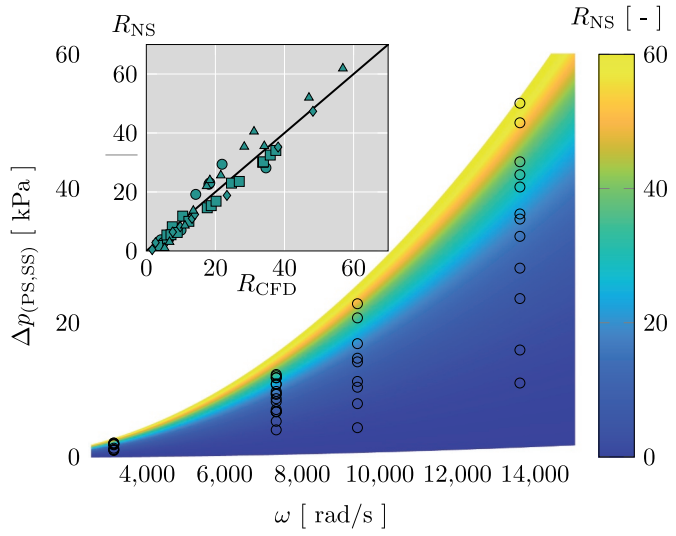

Fig. 14. Model results and validation for the points of highest $\Delta p_{(PS,SS)}$ per running point. Color: radial velocity and local blade loading vs. momentum ratio R_{NS}; Dots: simulated rotational velocity and maximum local blade loading in the exducer for each running point; Small: Momentum ratio R_{NS} vs. momentum ratio R_{CFD} at highest local blade loading close to the tip.

5.3. Tip leakage velocity fitting

As in Eq. (2) many tip leakage loss correlations are based on the positive tip leakage velocity. By using Eq. (7) and correlating the effective inflow length with:

$$\Delta\theta_{eff.} = c \cdot (Re_{-})^{b}. \tag{23}$$

good fittings have been achieved with CFD data for modeled $\bar{w}_{tip,\delta,+}$ as it can be seen in Fig. 15. Here, $\Delta\theta_{eff.}$ does only depend on the negative Reynolds number as it has been defined in Eq. (19) and the same exponent ($b = 1.23$) that has been found for the momentum ratio can be applied. This way only one additional coefficient is necessary. The factor c has been fitted with 2332. Also here, $\Delta\theta_{eff.}$ has a similar function as a discharge coefficient.

5.4. Incidence flow analysis

As highlighted before, incidence flow has significant influence on the momentum ratio in the rotor inlet and contributes to the tip leakage loss itself. Hence, the evaluation of this mixed flow effect can be of high

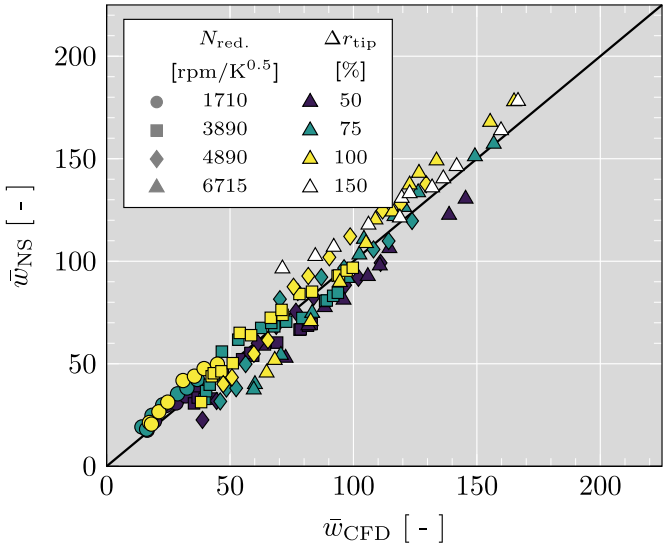

Fig. 15. Fitting of $\bar{w}_{tip,\vartheta,+}$: model vs. CFD data.

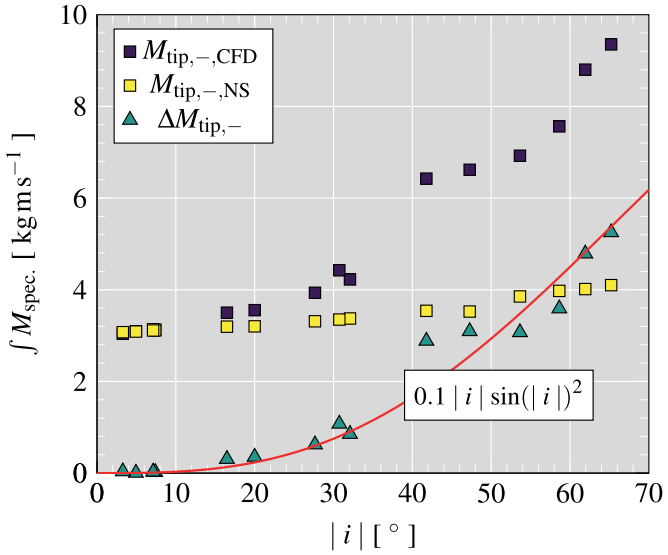

Fig. 16. Chordwise integral of negative momentum and difference between CFD and model at 3890 rpm/K$^{0.5}$ and 100% tip gap opening.

importance. Taking advantage of the already found correlation for the momentum ratio and positive leakage velocity, the mean negative velocity and momentum driven by shroud friction can be found by Eqs. (24) and (25) respectively.

$$\bar{w}_{tip,\vartheta,-,NS} = \sqrt{\frac{\rho_+}{\rho_-}\frac{\bar{w}^2_{tip,\vartheta,+,NS}}{R_{NS}}} \tag{24}$$

$$\bar{M}_{tip,-,NS} = \rho \bar{w}^2_{tip,\vartheta,-,NS} \tag{25}$$

In Fig. 16 the chordwise integral of this momentum has been compared with the same value from the CFD results for the entire speedline of 3890 rpm/K$^{0.5}$, since this speed has running points from very low incidence to high negative incidence. Calculating the deviation between both shows clearly values close to zero when the inflow incidence is low and rising values towards higher negative incidence. This highlights again the validity of the before derived correlations for friction-driven and pressure-driven flow. Although the momentum ratio R_{NS} is worse predicted at low cord length in Fig. 11, the overall fitting is capable of characterizing both flow effects in this zone, where incidence is important. Hence, the found correlations can be used to separate these flow phenomena and to analyze the incidence flow. It is worth highlighting that the incidence-driven momentum reaches the same magnitude as the friction-driven momentum predicted by Eq. (25) when the incidence becomes high. This again proofs the importance of incidence flow for the tip leakage flow. The filtered incidence flow momentum can be fitted in good quality with $0.1|i|\sin(|i|)^2$ as it has been demonstrated in Fig. 16. Here $\sin(|i|)^2$ is clearly related with the tangential part of the inflow momentum. The factor $0.1|i|$ is assumed to be related with geometric measures like the tip gap height and the distribution of γ in the passage inlet in combination with aerodynamic interactions with friction-driven and pressure-driven flow.

6. Conclusions

The main conclusions of the work are highlighted as follows:

1. Steady state simulations at four different reduced speeds with three different tip gap variations (four tip gap variations at highest speed) have been executed in a wide range of operating conditions.
2. Incidence flow has been identified to influence the tip leakage specific mass flow and momentum. While it reduces the pressure induced specific mass flow in the tip gap at low chord length, the incidence inflow leads to an increase of inverse directed specific mass flow and momentum, which causes a further entropy rise.
3. The ratio of friction and pressure ratio driven momentum has been analyzed and it has been stated that available correlations are not capable of doing quantitative conclusions of tip leakage flow over the chord length and neither qualitative conclusions of geometry changes.
4. A new correlation to calculate the momentum ratio based on the Navier Stokes Equation has been derived. The equation inherent flow length, here interpreted as effective flow length, has been fitted dependent on the ratio of Reynolds numbers build for friction driven and pressure driven flow $\frac{Re_-}{Re_+^{1/6}}$ for all analyzed running conditions at design and off-design, from low to high rotational speed, and for varied geometry.
5. It has been demonstrated that the tip leakage flow reacts sensitively on small changes in the tip blade loading when operating close to design conditions. With slightly higher pressure between SS and PS the momentum ratio and related losses can increase significantly.
6. A correlation has been found to fit the pressure driven velocity, which allows to calculate the impact of friction momentum and to analyze the impact of the incidence flow momentum.
7. Derived correlations can directly been used in efficiency extrapolation models that rely on tip leakage velocities or momentums.
8. Consistent model fitting allows to fit the correlation with data of only one tip gap geometry and to extrapolate towards other geometries. This can be important when cold geometries are numerically assessed.
9. As demonstrated the correlations can further been used to analyze mixed flow phenomena in the tip leakage flow. Also, found trends can be of interest for turbocharger turbine designer.
10. The physical basis of presented characterization might allow an application for axial turbine tip leakage flow in the future.

Acknowledgments

The work has been partially supported by FEDER and the Spanish Ministry of Economy and Competitiveness through grant number TRA2016-79185-R. The authors would also like to acknowledge the Research and Development Aid Program PAID-01-16 of the Universitat Politecnica de Valencia, Spain.

Authors want to thank intern Niki Wilms for his valuable assistance in the data processing.

References

Baines, N., 1998. A meanline prediction method for radial turbine efficiency. IMECHE Conference Transactions. Vol. 11. Mechanical Engineering Publications, pp. 45–56.

Baines, N., 2006. Radial turbine design. Axial and Radial Turbines. Concepts NREC.

Borutzky, W., Barnard, B., Thoma, J., 2002. An orifice flow model for laminar and turbulent conditions. Simul. Modell. Pract. Theory 10 (3), 141–152. https://doi.org/10.1016/S1569-190X(02)00092-8.

Dambach, R., Hodson, H., 2001. Tip leakage flow in a radial inflow turbine with varying gap height. J. Propul. Power 17 (3), 644–650. https://doi.org/10.2514/2.5791.

Dambach, R., Hodson, H., Huntsman, I., 1998. An experimental study of tip clearance flow in a radial inflow turbine. ASME. Turbo Expo: Power for Land, Sea, and Air, Volume 1: Turbomachinery ( ):V001T01A110. American Society of Mechanical Engineershttps://doi.org/10.1115/98-GT-467.

Dambach, R., Hodson, H., Huntsman, I., 2002. Tip-leakage flow: a comparison between small axial and radial turbines. Micro-Turbine Generators 97.

Galindo, J., Fajardo, P., Navarro, R., García-Cuevas, L., 2013. Characterization of a radial turbocharger turbine in pulsating flow by means of CFD and its application to engine modeling. Appl. Energy 103, 116–127. https://doi.org/10.1016/j.apenergy.2012.09.013.

Galindo, J., Hoyas, S., Fajardo, P., Navarro, R., 2013. Set-up analysis and optimization of CFD simulations for radial turbines. Eng. Appl. Comput. Fluid Mech. 7 (4), 441–460. https://doi.org/10.1080/19942060.2013.11015484.

Galindo, J., Tiseira, A., Navarro, R., López, M., 2015. Influence of tip clearance on flow behavior and noise generation of centrifugal compressors in near-surge conditions. Int. J. Heat Fluid Flow 52, 129–139. https://doi.org/10.1016/j.ijheatfluidflow.2014.12.004.

Kammeyer, J., Natkaniec, C., Seume, J.R., 2010. Influence of tip-gap losses on the stage efficiency of downsizing turbocharger turbines. 9th International Conference on Turbochargers and Turbocharging,19-20 May, London.

Kammeyer, J., Natkaniec, C., Seume, J.R., 2010. Tip leakage in small radial turbines: Optimum tip-gap and efficiency loss correlations. ASME Turbo Expo 2010: Power for Land, Sea, and Air. American Society of Mechanical Engineers, pp. 391–401. https://doi.org/10.1115/GT2010-22680.

Menter, F.R., 1994. Two-equation eddy-viscosity turbulence models for engineering applications. AIAA J. 32 (8), 1598–1605. https://doi.org/10.2514/3.12149.

Menter, F.R., Langtry, R., Hansen, T., 2004. CFD simulation of turbo-machinery flows-verification, validation and modeling. European Congress on Computational Methods in Applied Sciences and Engineering, ECCOMAS.

Peacock, R., 1982. A review of turbomachinery tip gap effects: part 1: cascades. Int. J. Heat Fluid Flow 3 (4), 185–193. https://doi.org/10.1016/0142-727X(82)90017-0.

Peacock, R., 1983. A review of turbomachinery tip gap effects: part 2: rotating machinery. Int. J. Heat Fluid Flow 4 (1), 3–16. https://doi.org/10.1016/0142-727X(83)90019-X.

Regulation (EC), 2007. No 715/2007 of the european parliament and of the council of 20 june 2007 on type approval of motor vehicles with respect to emissions from light passenger and commercial vehicles (euro 5 and euro 6) and on access to vehicle repair and maintenance information (text with EEA relevance). Off. J. Eur. Union 50, 1–16.

Romagnoli, A., Martinez-Botas, R., 2011. Performance prediction of a nozzled and nozzleless mixed-flow turbine in steady conditions. Int. J. Mech. Sci. 53 (8), 557–574. https://doi.org/10.1016/j.ijmecsci.2011.05.003.

Salameh, G., Chesse, P., Chalet, D., 2016. Different measurement techniques for wider small radial performance maps. Exp. Tech. 40 (6), 1511–1525. https://doi.org/10.1007/s40799-016-0107-8.

Serrano, J.R., Arnau, F.J., García-Cuevas, L.M., Dombrovsky, A., Tartousi, H., 2016. Development and validation of a radial turbine efficiency model at extreme off-design conditions. Energy Convers. Manage. https://doi.org/10.1016/j.enconman.2016.09.032.

Serrano, J.R., García-Cuevas, L.M., Inhestern, L.B., Mai, H., Rinaldi, A., Miguel-Sanchez, A., 2017. Methodology to evaluate turbocharger turbine performance at high blade to jet speed ratio under quasi adiabatic conditions. ASME. Turbo Expo: Power for Land, Sea, and Air, Volume 8: Microturbines, Turbochargers and Small Turbomachines; Steam Turbines ( ):V008T26A004. American Society of Mechanical Engineershttps://doi.org/10.1115/GT2017-63360.

Serrano, J.R., Gil, A., Navarro, R., Inhestern, L.B., 2017. Extremely low mass flow at high blade to jet speed ratio in variable geometry radial turbines and its influence on the flow pattern: a CFD analysis. ASME. Turbo Expo: Power for Land, Sea, and Air, Volume 8: Microturbines, Turbochargers and Small Turbomachines; Steam Turbines (~):V008T26A005. American Society of Mechanical Engineershttps://doi.org/10.1115/GT2017-63368.

Serrano, J.R., Navarro, R., García-Cuevas, L.M., Inhestern, L.B., 2018. Method for non-dimensional tip leakage flow characterization in radial turbines. ASME Turbo Expo in Oslo. American Society of Mechanical Engineershttps://doi.org/10.1115/GT2018-76490.

Serrano, J.R., Navarro, R., García-Cuevas, L.M., Inhestern, L.B., 2018. Turbocharger turbine rotor tip leakage loss and mass flow model valid up to extreme off-design conditions with high blade to jet speed ratio. Energy 147, 1299–1310. https://doi.org/10.1016/j.energy.2018.01.083.

Serrano, J.R., Olmeda, P., Arnau, F.J., Dombrovsky, A., 2014. General procedure for the determination of heat transfer properties in small automotive turbochargers. SAE Int. J. Engines 8 (1). https://doi.org/10.4271/2014-01-2857.

Serrano, J.R., Olmeda, P., Tiseira, A., García-Cuevas, L.M., Lefebvre, A., 2013. Theoretical and experimental study of mechanical losses in automotive turbochargers. Energy 55 (0), 888–898. https://doi.org/10.1016/j.energy.2013.04.042.

Serrano, J.R., Tiseira, A., García-Cuevas, L.M., Inhestern, L.B., Tartoussi, H., 2017. Radial turbine performance measurement under extreme off-design conditions. Energy 125, 72–84. https://doi.org/10.1016/j.energy.2017.02.118.

Simpson, A.T., Spence, S.W.T., Watterson, J.K., 2009. A comparison of the flow structures and losses within vaned and vaneless stators for radial turbines. J. Turbomach. 131. https://doi.org/10.1115/1.2988493.

Terdich, N., 2015. Impact of Electrically Assisted Turbocharging on the Transient Response of an Off-Highway Diesel Engine. Imperial College London.

Yaras, M., Sjolander, S., 1992. Prediction of tip-leakage losses in axial turbines. ASME J. Turbomach. 114 (1), 204–210. https://doi.org/10.1115/90-GT-154.